Scalar mixing in homogeneous isotropic turbulence: A numerical study

Michel Orsi,[1] Lionel Soulhac,[2] Fabio Feraco,[2,3] Massimo Marro,[2] Duane Rosenberg,[4] Raffaele Marino,[2] Maurizio Boffadossi,[1] and Pietro Salizzoni[2]

[1]*Department of Aerospace Engineering, Politecnico di Milano, 34 via La Masa, 20158 Milano, Italy*

[2]*Laboratoire de Mécanique des Fluides et d'Acoustique, University of Lyon, CNRS UMR 5509, École Centrale de Lyon, INSA Lyon, Université Claude Bernard, 36 Avenue Guy de Collongue, 69134 Écully, France*

[3]*Dipartimento di Fisica, Università della Calabria, Italy*

[4]*1401 Bradley Drive, Boulder 80305, Colorado, USA*

(Received 19 April 2020; accepted 3 March 2021; published 19 March 2021)

The understanding of the mechanics of turbulent dispersion is of primary importance in estimating the effects of mixing processes involved in a variety of events playing a significant role in our daily life. This motivates research on the characterization of statistics and the complex temporal evolution of passive scalars in turbulent flows. A key aspect of these studies is the modeling of the probability density function (PDF) of the passive scalar concentration and the identification of its link with the mixing properties. In order to investigate the dynamics of passive scalars as observed in nature and in laboratory experiments, we perform here direct numerical simulations of a passive tracer injected in the stationary phase of homogeneous isotropic turbulence flows in a setup mimicking the evolution of a fluid volume in the reference frame of the mean flow. In particular, we show how the gamma distribution proves to be a suitable model for the PDF of the passive scalar concentration and its temporal evolution in a turbulent flow throughout the different phases of the mixing process. Then, assuming a gamma distribution, we develop a simple mixing model by which we can estimate a mixing timescale, which regulates the decay rate of the intensity of the concentration fluctuations.

DOI: 10.1103/PhysRevFluids.6.034502

I. INTRODUCTION

Turbulent dispersion and mixing of passive scalars are ubiquitous in nature. As is well known, the turbulent character of the high Reynolds (Re) number flows is reflected on the fluctuations of the passive scalar concentration occurring over a wide range of spatial and temporal scales [1]. The statistical characterization of these fluctuations is essential for the modeling of several processes occurring in industrial, biological, and environmental flows (see Fig. 1 as examples). To this aim, over the years this issue has been tackled by several authors considering a large variety of flow configurations [2–8].

In a number of applications of interest in physics, chemistry, biology, and engineering, a key aspect is the prediction of the spatial variability of the one-point probability density function (PDF) of the scalar field. Previous works have shown that, depending on the flow configuration, this can be modeled by different distributions [2–9], including the Weibull, the lognormal, and the gamma distributions. Notably, the latter was shown to be a suitable model for both dispersion and mixing in internal flows [2–7] and in the atmosphere [6–8,10–14].

The present paper aims at further exploring the above features, through the investigation of concentration statistics and mixing in a framework mimicking the evolution of the passive scalar in a homogeneous isotropic turbulent flow. To this purpose, we performed direct numerical simulations

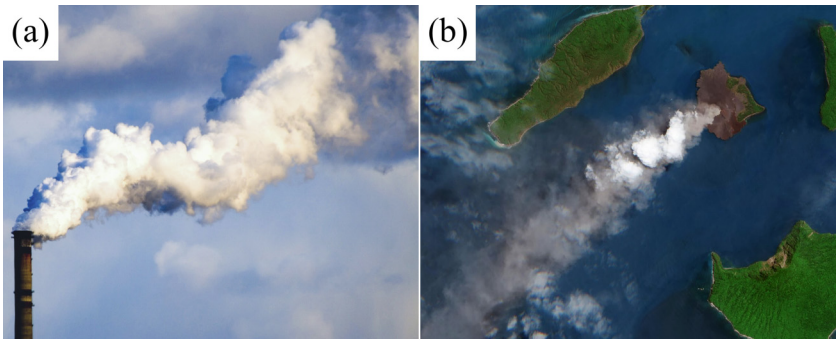

FIG. 1. (a) Plume generated by a chimney (i.e., an elevated continuous source in a nonisotropic and nonhomogeneous turbulent flow field); (b) volcanic ash and steam in the Sunda Strait released by the Anak Krakatau volcano in Indonesia 3 months before its eruption in December 2018.

(DNSs) of a stationary turbulent velocity field (with zero mean) where a puff of passive scalar was released and let evolve to get insights on its diffusion and mixing properties (Sec. II). In Sec. III concentration statistics and PDF computed on the pointwise simulated fields were first checked to ascertain their reliability and then linked to the main mechanisms involving the mixing. Finally, we discuss the consistency between spatial statistics computed by the DNS (seeing the puff as evolving in a Lagrangian framework moving with the mean flow) and the temporal statistics based on one-point wind-tunnel measurements (Sec. IV).

II. NUMERICAL SIMULATION

In order to investigate the dispersion and mixing of a passive scalar in homogeneous isotropic turbulence (HIT), the Navier-Stokes equations for an incompressible fluid together with the convection-diffusion equation for the concentration are integrated by means of the geophysical high-order suite for turbulence code [15], a highly parallelized (hybrid MPI-OPENMP) pseudospectral framework with second-order explicit Runge-Kutta time stepping. The Navier-Stokes equations have been integrated on a cubic grid of 512^3 points (corresponding to a box whose linear size in adimensional units is $L_0 = 2\pi$) with periodic boundary conditions. A stochastic forcing $\mathbf{F}$ was used to inject energy into the velocity field to achieve and maintain a statistically stationary state. The forcing is random in time and isotropic in Fourier space with the energy being injected at large scales in a spherical shell of wave-numbers $2 \leqslant |k_i| \leqslant 3$. A puff of a passive scalar modeled with a Gaussian concentration peaked in the center of the box is injected at an arbitrary time in the statistically stationary state of the simulation and is let to diffuse. The full system of equations implemented is reported here

$$\begin{aligned} \boldsymbol{\nabla} \cdot \mathbf{u} &= 0, \\ \partial_t \mathbf{u} + (\mathbf{u} \cdot \boldsymbol{\nabla})\mathbf{u} &= -\boldsymbol{\nabla} p + \mathbf{F} + \frac{1}{\mathrm{Re}} \nabla^2 \mathbf{u}, \\ \partial_t c + \mathbf{u} \cdot \boldsymbol{\nabla} c &= \frac{1}{\mathrm{Pr}\,\mathrm{Re}} \nabla^2 c, \end{aligned} \tag{1}$$

$\mathbf{u}$ being the velocity field, p is the pressure, and c is the passive scalar concentration. The DNS governing parameters are the Prandtl (Pr) and the Reynolds (Re) numbers. The former, defined as $\mathrm{Pr} \equiv \nu/\kappa$, is set equal to 1 (being ν and κ the kinematic viscosity and the diffusivity, respectively). The latter is instead $\mathrm{Re} \equiv \frac{UL}{\nu}$, where $U = \sqrt{3\sigma_u^2}$ (being $\sigma_u^2 = \sigma_v^2 = \sigma_w^2 \sim 1$ the variances of the three velocity components averaged over the computational domain) and $L = \frac{2\pi}{k_j \sim 2.5}$, respectively, are the characteristic velocity and the integral length scale of the background fluid (the latter being

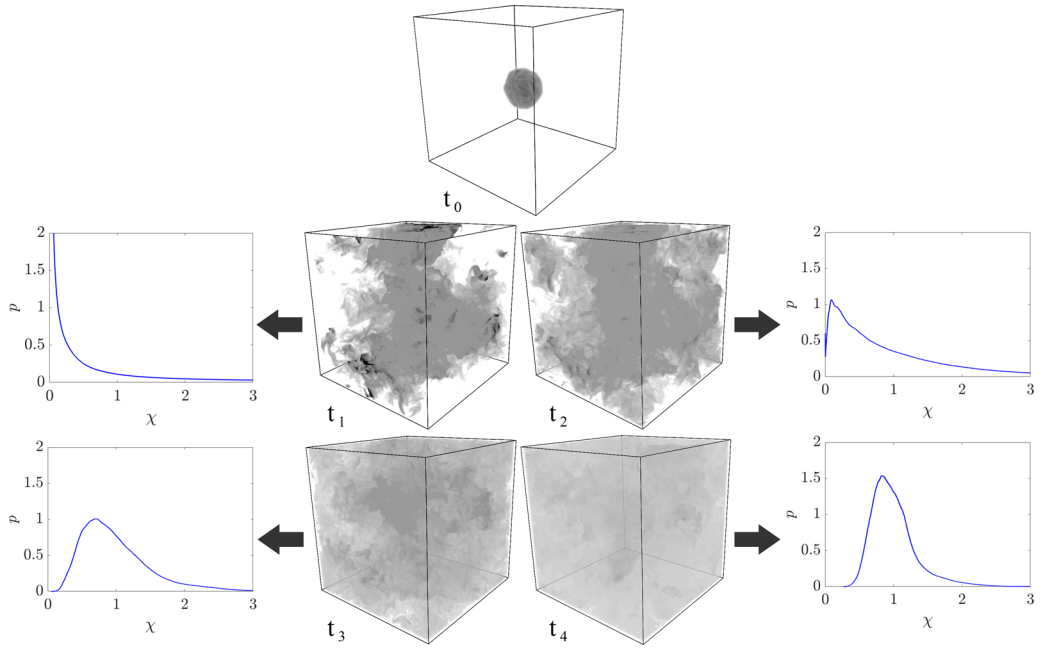

FIG. 2. Visualization of different instants of the DNS solutions and corresponding concentration PDFs: at the top (t_0), the initial condition can be observed; at the bottom right (t_4), the passive scalar homogenizes itself within the box.

estimated as the scale at which energy is injected into the system). Based on these quantities we can estimate the turnover time $t^* \equiv L/U$, the characteristic timescale of the simulation, whose total extension is about $10t^*$. The simulations have been performed at two Reynolds numbers, namely, 3000 and 3500. For $\mathrm{Re} = 3000$ the Kolmogorov length scale is $\eta = (\nu^3/\varepsilon)^{1/4} = 8.15 \times 10^{-3}$ (ε is the turbulent kinetic-energy dissipation rate), which is three orders of magnitude lower than the integral length scale ($\eta/L = 3.24 \times 10^{-3}$). Note that the (periodic) boundary conditions induce the concentration averaged over the domain ($\overline{c}$) to be constant throughout the simulation duration.

III. RESULTS

The concentration statistics provided by the DNS results allow the temporal evolution of the mixing process to be investigated. To that purpose, we focus on two main statistical indicators: the shape of the PDF of the spatial distribution of the concentration and the (volume-averaged) concentration fluctuations intensity i_c (defined as the ratio between the standard deviation of the concentrations σ_c and $\overline{c}$). The first feature that is worth noting is the strict connection between the temporal evolutions of these two indicators.

Notably, once excluded the early transient of the simulation (lasting less than one turnover time t^*) during which the system progressively "loses memory" of the initial concentration distribution (Fig. 2, t_0), we can identify two main stages of the process by linking the shape of the PDFs (Fig. 2) to i_c (Fig. 3). To allow the reader to suitably capture this connection between the concentration PDF and i_c, we provided a movie as Supplemental Material [16]. During the first phase, starting at the inflection point of i_c, the scalar is progressively transported throughout the domain as shown in Fig. 2 at t_1. This stage presents specific features: (i) i_c is larger than 1, (ii) the concentration PDF is characterized by a large number of zero values (mostly distributed at the edge of the evolving puff), and (iii) it approximates an exponential-like shape. The second phase begins when the domain

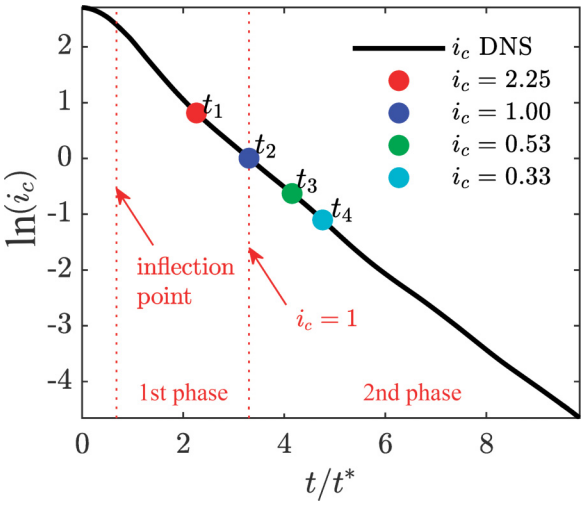

FIG. 3. Behavior of the concentration fluctuations intensity i_c over time: four instants t_1, t_2, t_3, and t_4 are highlighted.

gets completely filled by the passive scalar (Fig. 2 at t_2) and $i_c = 1$ (Fig. 3), and it is mostly characterized by the diffusion. During this stage the scalar field progressively homogenizes (as shown in Fig. 2 at t_3) and the concentration PDFs assume a lognormal-like shape. The increasing scalar homogenization (Fig. 2 at t_4) induces a further transition of the PDFs towards a clipped Gaussian [13].

The results of the simulations performed with two different Reynolds numbers (i.e., Re = 3000 and Re = 3500) did not show any relevant difference one to the other. In what follows we will, therefore, present results for the case of Re = 3000. Concentration statistics recover those obtained with the smaller blob as $t/t^* > 2$.

A. Concentration PDF

In order to identify the statistical distribution showing the best agreement with the presented numerical results, we tested different models for the scalar PDF. To do this, we, therefore, computed the PDF of the concentration for each time step. The agreement between the PDFs obtained from the DNS and the analytical model distributions is estimated here using the Kullback-Leibler divergence D_{KL} [17], defined as

$$D_{KL}(p \parallel q) \equiv -\sum p \log_2 \left(\frac{p}{q}\right), \tag{2}$$

where p is the PDF from the DNS and q is the distribution assumed as a model. According to this definition, the best agreement is observed when $p/q \to 1$, i.e., for $D_{KL} \to 0$.

We tested three different distributions which have been proposed over the years as suitable models for the passive scalar concentration PDF within a turbulent flow [2–9]. These are as follows:

(1) the gamma distribution,

$$p(\chi|\lambda, \theta) = \frac{1}{\Gamma(\lambda)\theta}\left(\frac{\chi}{\theta}\right)^{\lambda-1} \exp\left(-\frac{\chi}{\theta}\right), \tag{3}$$

where χ is the sample space variable for the concentration, $\Gamma(\cdot)$ is the Gamma special function [18], and $\lambda = i_c^{-2}$ and $\theta = \sigma_c^2/\overline{c}$ are the shape and scale parameters, respectively. It is worth noting that normalizing the distribution as $\chi' \equiv \chi/\overline{c}$ allows us to reduce the problem to only the shape parameter λ [2,19,20];

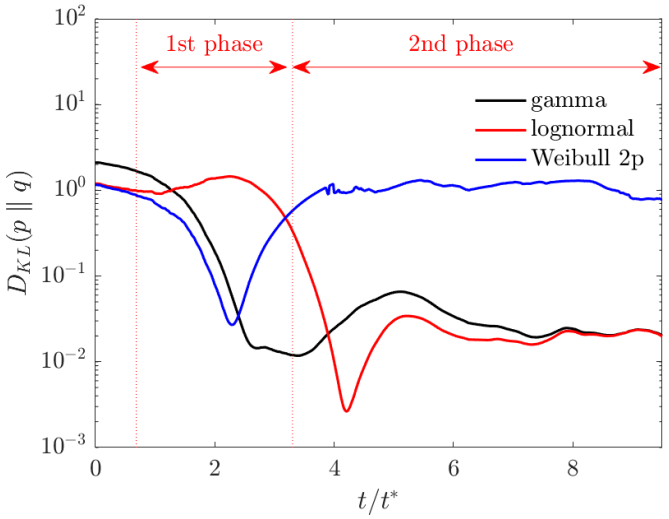

FIG. 4. Kullback-Leibler divergence of the PDF from the DNS results (semilogarithmic plot): comparison among the gamma, the lognormal, and the Weibull $2p$ distributions. The two vertical dashed lines indicate different phases of the mixing processes as defined in Sec. III. The KL divergence of the gamma distribution presents a good overall behavior, and it is the most suitable choice for modeling the scalar-field PDF for all the time steps.

(2) the lognormal distribution,

$$p(\chi|\mu_l,\sigma_l) = \frac{1}{\chi\sigma_l\sqrt{2\pi}}\exp\left[-\frac{(\ln\chi-\mu_l)^2}{2\sigma_l^2}\right] \tag{4}$$

for $\chi > 0$ and with the parameters,

$$\mu_l = \ln\left(\overline{c}^2/\sqrt{\sigma_c^2+\overline{c}^2}\right),$$
$$\sigma_l = \sqrt{\ln\left(\sigma_c^2/\overline{c}^2+1\right)}, \tag{5}$$

(3) the Weibull $2p$ distribution,

$$p(\chi|a_w,b_w) = \frac{b_w}{a_w}\left(\frac{\chi}{a_w}\right)^{b_w-1}\exp\left[-\left(\frac{\chi}{a_w}\right)^{b_w}\right], \tag{6}$$

being a_w and b_w the scale and the shape parameters, respectively, set as

$$i_c^2 + 1 - \frac{\Gamma\left(1+\frac{2}{b_w}\right)}{\left[\Gamma\left(1+\frac{1}{b_w}\right)\right]^2} = 0,$$
$$a_w = \frac{\overline{c}}{\Gamma\left(1+\frac{1}{b_w}\right)}. \tag{7}$$

We point out that the computation of b_w requires to solve the nonlinear Eq. (8). We mention that for practical application the shape parameters can be conveniently approximated as $b_w \approx (1/i_c)^{1.086}$ e.g., Ref. [21].

As shown in Fig. 4, close to t_0 the lognormal distribution is not appropriate since it is not able to reproduce the effects of the meandering process in the near field as observed close to the scalar source in wind-tunnel experiments. Conversely, it provides accurate estimates of the scalar PDF

after the homogenization process induced by the relative dispersion. The Weibull $2p$ distribution performs suitable approximations of the concentration PDF in the near field, whereas it fails to model the distribution of the scalar at large values of t/t^*.

The gamma distribution shows a more accurate overall behavior providing a good agreement with the numerical solutions both in the near and in the far field. Such behavior suggests that the gamma PDF is a robust model being able to replicate the main features of the mixing process over the entire DNS.

B. Mixing

As a second step, we discuss here the implications of a mixing process due to the interaction of pollutant particles, assuming, based on the results presented in the previous paragraph, that the PDF of the concentration within our reference volume is a gamma distribution. In order to analyze the mixing process, we focus on the fluctuations intensity i_c, that progressively goes to zero. Note that because of the imposed boundary conditions (Sec. II), the decay of i_c is entirely due to the reduction of the standard deviation σ_c since the spatially averaged concentration $\overline{c}(t)$ remains unaltered.

We represent the passive-scalar puff as constituted of an ensemble of "marked" fluid particles so that the mixing process is modeled as a "discrete" phenomenon resulting by the interaction of pairs of marked fluid particles. This is a classical pattern in PDF methods for the prediction of concentration fluctuations (referred to as micromixing models) implemented in Lagrangian one-particle dispersion models [9,22]. In this kind of model, each fluid particle exchanges mass with the surrounding particles and, as a consequence, the concentration statistics defined by an ensemble of neighboring particles evolve in time. Then, following this analogy, the concentrations of the fluid particles can be considered as single realizations of the same random variable whose statistical behavior is modeled by a distribution that we assume to be a gamma PDF. The two fluid particles, denoted as 1 and 2, exchange mass each other so that the temporal evolution of their concentrations develops as a system of two ordinary differential equations,

$$\begin{aligned} \frac{dc_1}{dt} &= -\frac{c_1 - c_2}{\tau_m}, \\ \frac{dc_2}{dt} &= -\frac{c_2 - c_1}{\tau_m}, \end{aligned} \tag{8}$$

here τ_m is the characteristic timescale of the mixing process. The solution of the system above in the time-interval $[t',\ t' + \Delta t]$ is as follows:

$$\begin{aligned} c_1(t' + \Delta t) &= (1 - \alpha)c_1(t') + \alpha c_2(t'), \\ c_2(t' + \Delta t) &= \alpha c_1(t') + (1 - \alpha)c_2(t'), \end{aligned} \tag{9}$$

where

$$\alpha \equiv \frac{1}{2}\left[1 - \exp\left(-2\frac{\Delta t}{\tau_m}\right)\right]. \tag{10}$$

Generalizing this approach to any pair of fluid particles i and j within the domain, we conclude that predicting the effect of mixing is equivalent to estimate the PDF of a new random variable c_k given by a weighted sum of c_i and c_j,

$$c_k(t' + \Delta t) = (1 - \alpha)c_i(t') + \alpha c_j(t'). \tag{11}$$

The PDF of c_k is then given by the convolution of the PDFs for c_i and c_j. Since $c_i(t')$ and $c_j(t')$ are both distributed according to the same gamma PDF $p(\lambda, \theta)$, we have that

$$\begin{aligned} (1 - \alpha)c_i(t') \quad &\text{follows } p_i[\lambda, (1 - \alpha)\theta], \\ \alpha c_j(t') \quad &\text{follows } p_j(\lambda, \alpha\theta). \end{aligned} \tag{12}$$

As far as we are aware, simple expressions for the convolution of two gamma distributions having different scale parameters [as in Eq. (13)] are not known. Moschopoulos [23] and Sim [24] provided the exact convolution as a sum of infinite terms, and Mathai [25] and Akkouchi [26] proposed some complicated formulas. An alternative approach was investigated in Stewart *et al.* [27] who showed that the sum of gamma PDFs is suitably approximated by a gamma distribution if the scale parameters differ no more than a factor of 10, and the shape parameters are not below 0.1. In our case these conditions are generally satisfied. The first condition is fulfilled for $\Delta t \geqslant 0.2\,\tau_m$, and the second one is fulfilled for $i_c \lesssim 3.2$. Therefore, the PDF $p_k(\lambda_k,\,\theta_k)$ of c_k [Eq. (11)] is suitably approximated as a gamma distribution [27], and its scale and shape parameters can be determined by computing mean and variance as follows:

$$\begin{aligned}
\overline{c}_k &= \lambda_k\theta_k \\
&= \lambda(1-\alpha)\theta + \lambda\alpha\theta \\
&= \lambda\theta, \\
\sigma_{c,k}^2 &= \lambda_k\theta_k^2 = \lambda(1-\alpha)^2\theta^2 + \lambda\alpha^2\theta^2 \\
&= \lambda\theta^2[(1-\alpha)^2 + \alpha^2], \\
\theta_k &= \frac{\sigma_{c,k}^2}{\overline{c}_k} \\
&= \theta[\alpha^2 + (1-\alpha)^2], \\
\lambda_k &= \frac{\overline{c}_k^2}{\sigma_{c,k}^2} \\
&= \frac{\lambda}{\alpha^2 + (1-\alpha)^2}.
\end{aligned} \tag{13}$$

As a consequence of the mixing process, the first two moments of the concentration PDF evolve as (dropping the indices for clarity),

$$\begin{aligned}
\overline{c}(t' + \Delta t) &= \overline{c}(t'), \\
\sigma_c^2(t' + \Delta t) &= \beta\sigma_c^2(t'),
\end{aligned} \tag{14}$$

where

$$\beta \equiv \alpha^2 + (1-\alpha)^2 = \frac{1}{2}\left[1 + \exp\left(-4\frac{\Delta t}{\tau_m}\right)\right]. \tag{15}$$

Performing a limited development of this process for short intervals and neglecting the higher-order terms, we obtain the evolution of the characteristics of the distribution between t' and $t' + \Delta t$,

$$\begin{aligned}
\overline{c}(t' + \Delta t) &= \overline{c}(t') \\
\sigma_c^2(t' + \Delta t) &= \left(1 - 2\frac{\Delta t}{\tau_m}\right)\sigma_c^2(t').
\end{aligned} \tag{16}$$

Since Eq. (17) represents the incremental ratio of σ_c, we can write the time derivative of the concentration variance as

$$\lim_{\Delta t \to 0} \frac{\sigma_c^2(t' + \Delta t) - \sigma_c^2(t')}{\Delta t} = \frac{d\sigma_c^2}{dt} = -\frac{2}{\tau_m}\sigma_c^2, \tag{17}$$

which essentially expresses the dissipation rate of the scalar variance $\varepsilon_c \equiv -2\nu\langle\partial c'/\partial x_i\rangle^2$.

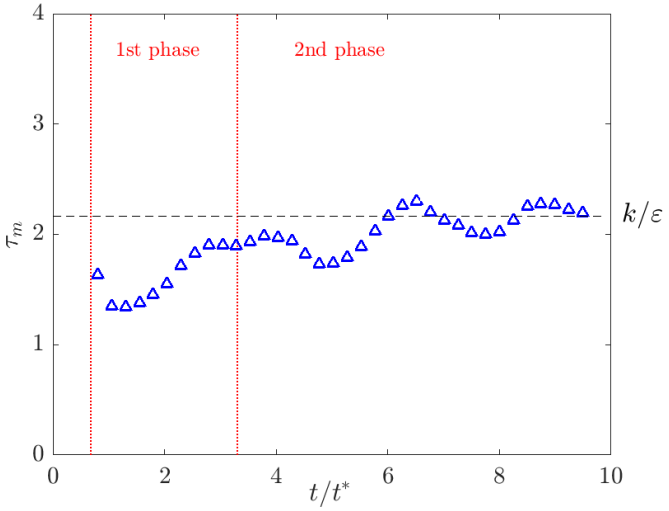

FIG. 5. Mixing timescale τ_m vs t/t^*. In the far field τ_m reaches the asymptotic value of k/ε.

The above expression can be integrated in order to obtain the temporal evolution of σ_c^2,

$$\sigma_c^2(t) = \sigma_c^2(0) \exp\left(-2\frac{t}{\tau_m}\right), \tag{18}$$

and, therefore,

$$\sigma_c(t) = \sigma_c(0) \exp\left(-\frac{t}{\tau_m}\right). \tag{19}$$

Since we have $\overline{c}(t) = \overline{c}(0)$, we finally obtain that the temporal decay of i_c evolves as

$$i_c(t) = i_c(0) \exp\left(-\frac{t}{\tau_m}\right), \tag{20}$$

showing that the assumption of the gamma distribution for the concentration PDF implies that the fluctuations intensity is given by a negative exponential, whose decay is governed by a typical mixing timescale.

The mixing timescale τ_m can be estimated from our numerical experiments by locally fitting Eq. (20) (i.e., over short intervals) with the DNS results for i_c, having τ_m as a free parameter (evolving in time). Once excluded the initial transient ($t/t^* < 1$), this timescale exhibits a smoothly growing trend in the first phase and oscillates around a constant value in the second phase. At later times, in the second phase of the simulation τ_m attains an asymptotic value equal to the dissipative timescale $\tau \equiv k/\varepsilon$ (where $k \equiv \frac{3}{2}\sigma_u^2$ is the turbulent kinetic energy and $\varepsilon \equiv 2\nu\langle s_{ij}s_{ij}\rangle$ is its dissipation rate) [28,29] as pointed out in Fig. 5. We highlight that the numerical results show that for large values of t/t^* the ratio $\tau/\tau_m \approx 1$, which is in agreement with the findings of other authors that reported values in the range of 0.3–1.56 for different configurations [22,30–33].

IV. ANALOGIES WITH WIND-TUNNEL RESULTS AND CROSS VALIDATION OF THE GAMMA MODEL

In Sec. III we have shown the temporal evolution of the normalized PDF of the passive scalar concentration and pointed out its link with the value of i_c: The shape of the PDF exhibits an exponential-like form as far as $i_c > 1$, and it abruptly changes shape for $i_c = 1$ and evolves as a Gaussian-like distribution as $i_c \to 0$. This same behavior, observed here adopting statistics over a

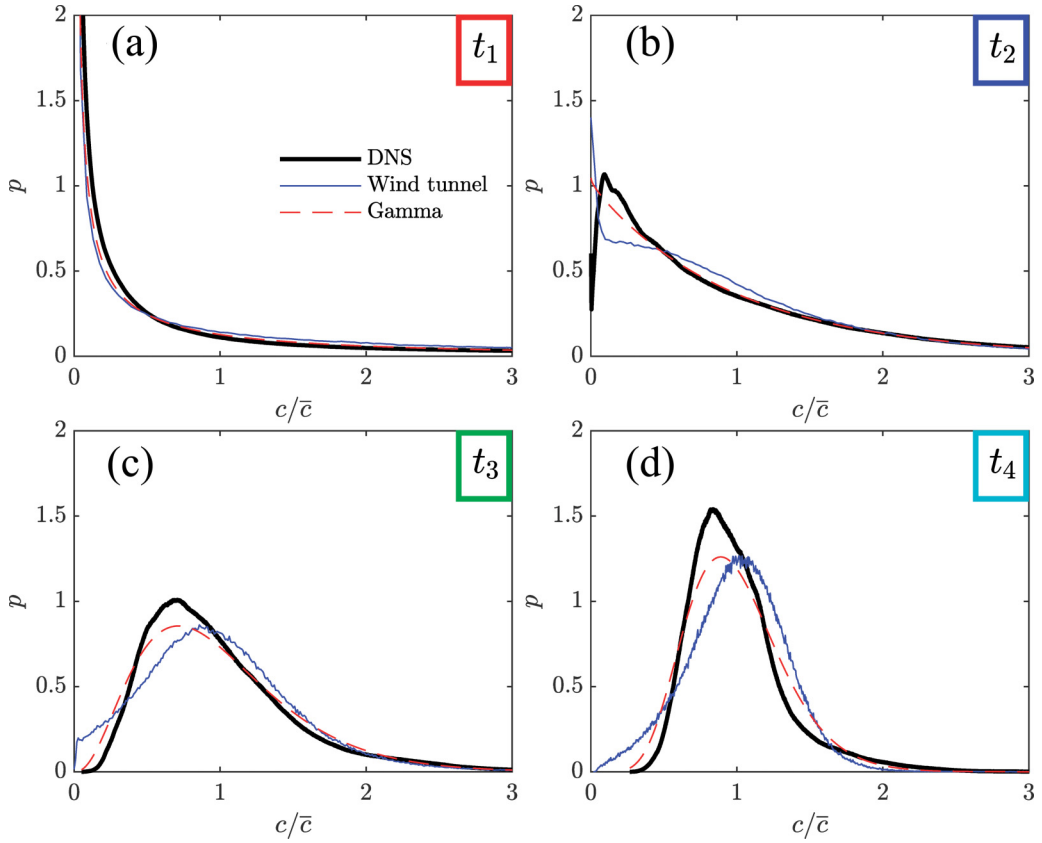

FIG. 6. Comparison between the normalized PDFs of the passive scalar concentration from the DNS, the wind-tunnel measurements by Nironi *et al.* [13], and the gamma distribution of Eq. (3) at decreasing values of i_c: (a) $i_c = 2.25$ at t_1, (b) $i_c = 1$ at t_2, (c) $i_c = 0.53$ at t_3, and (d) $i_c = 0.33$ at t_4.

control fluid volume for each time step, was observed in wind-tunnel experiments when analyzing one-point statistics obtained from concentration time series measured at a fixed location downwind a continuous scalar release in a turbulent boundary layer as described in Ref. [13]. Indeed, wind-tunnel experiments have shown that the statistics of the concentration of a continuous scalar plume in a boundary layer (i.e., a nonisotropic and nonhomogeneous velocity field) can be fully described by a gamma distribution as reported in Eq. (3).

In Fig. 6 we show a comparison between the present DNS results, the one-point wind-tunnel statistics performed by Nironi *et al.* [13] and the gamma distribution [Eq. (3)] for the same values of i_c (being t_1, t_2, t_3, and t_4 the same as in Fig. 3). Here, we can appreciate how the DNS solutions and the wind-tunnel measurements exhibit a similar behavior and that the gamma distribution can be assumed as a suitable model for both numerical and experimental PDFs. To explain this evidence from a phenomenological stand point, we can rely on the depiction in Fig. 7, proposing the analogy between the present DNS simulation of an unsteady decaying puff and the wind-tunnel results of a steady release of a passive scalar in a turbulent wall-bounded flow.

A peculiar aspect of the dispersion of localized atmospheric releases is the appearance of a meandering motion of the plume [12] due to the action of turbulent eddies larger than the plume size. The meandering highly affects the dispersion process in the near field of the source and is gradually attenuated moving away from it as the size of the plume increases under the action of the relative dispersion (due to eddies smaller than the puff size). As the relative dispersion finally induces the

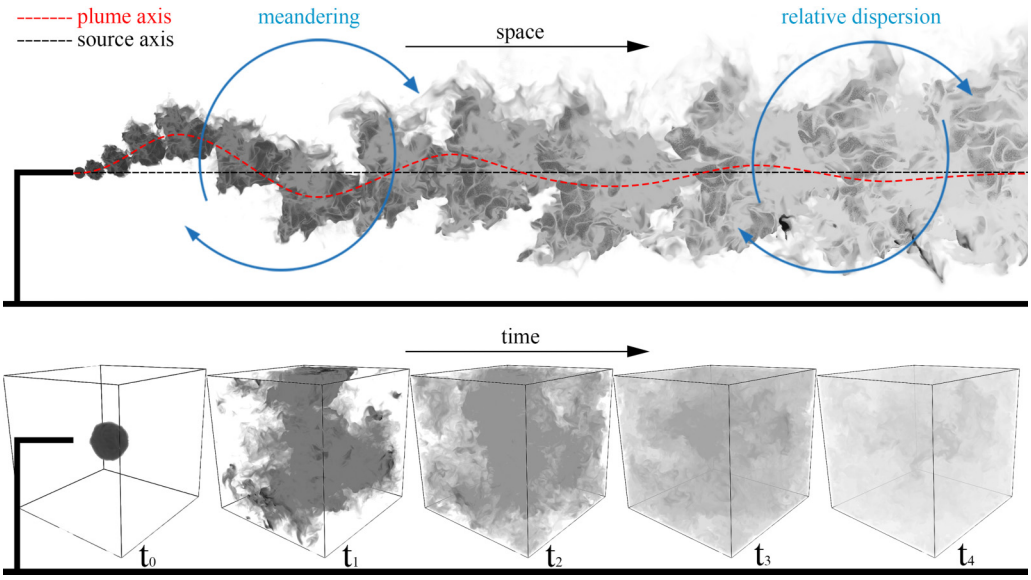

FIG. 7. Top panel: sketch of a plume as made of multiple puffs, the Eulerian approach. Bottom panel: numerical point of view, the Lagrangian approach. We observe the relationship between *space* and *time* in the two different approaches as well as the regions of *meandering* and *relative dispersion*.

plume size to exceed the size of the larger-scale structure of the flow, the plume meandering is suppressed. At first sight, we can consider that the transition between these two regimes occurs as i_c drops below 1, and the intermittency is suppressed in the core of the plume [13].

In the puff, at each time step, every point of the simulation domain can be considered as a possible realization of the plume along the source axis at a given distance from the source, in the equivalent reference wind-tunnel experiment. In other words, we can consider that the DNS results mimic the evolution of the scalar puffs released in the wind tunnel as they get translated horizontally by the mean flow whereas undergoing turbulent advection. Invoking the ergodicity of both numerical and experimental flows, we could, therefore, compare the spatial statistics computed on the simulation output (Fig. 7, bottom) with the single-point temporal statistics computed in the wind tunnel (Fig. 7, top). Thus, taking a specific instant of the DNS, the spatial statistics of the concentration over the entire simulation box would match the temporal statistics of the concentration signal measured at the corresponding position (always on the plume centreline, i.e., at the source height) in the wind-tunnel experiment. In this framework, the near-source meandering region in the experiments (Fig. 7, top panel) in which one-point statistics exhibit high intermittency, corresponds to the first phase of the DNS simulation (Fig. 7, bottom panel, t_1) in which the scalar has not filled the domain yet, and the spatial concentration statistics are affected by the presence of zero values of the concentration in part of it. Similarly, the far-field relative dispersion region in which the intermittency in the one-point statistics is suppressed, corresponds to the second phase of our DNS results (Fig. 7, bottom panel, t_3 and t_4) in which the scalar has filled the box and the mixing acts towards a complete homogenization of the concentration.

In the description of the dispersion process made so far, we adopted a jargon familiar to researchers working in the field of the atmospheric pollutant dispersion. Other researcher working reactive and nonreactive scalar mixing in turbulent flows adopt a different terminology to identify different regimes of the time evolution of the tracer distribution. According to this terminology, the second phase of our numerical simulations shows a behavior similar to that of the “confined mixture” regime in which, following Duplat and Villermaux [7], a self-convolution mechanism leads to a sequence of gamma distributions until complete mixing is reached. The dispersion in

the near-source region where the plume meanders in an unbounded environment has been instead referred as "ever dispersion mixture" by Duplat *et al.* [34]. The near-source region investigated by Duplat *et al.* [34] is, however, more similar to the initial transient of our simulations in which the concentration PDFs are not consistent with the gamma model (see Fig. 2 between t_0 and t_1), rather than what we referred to as the first phase where the gamma model actually holds. Similar considerations about the lack of accuracy of the gamma distribution as a model for the concentration PDFs very close to the release point were also presented by Sawford and Stapountzis [35] and Ardeshiri *et al.* [14].

V. CONCLUSIONS

We employed direct numerical simulations to investigate the passive-scalar dispersion and the related mixing processes within turbulent flows in a synergistic approach that involved the use of wind-tunnel measurements for the cross validation (numerical and experimental) of the gamma model for the scalar distribution concentration. In particular, we simulated a single puff in homogeneous isotropic turbulence in a cubic domain with a regular grid and periodic boundary conditions.

Focus of our paper is the analysis of the evolution in time of the spatial statistics of the scalar concentration within a fluid volume as seen in a reference frame following the mean flow. As first step, we tested the capability of different model distributions (the gamma, the lognormal, and the Weibull $2p$) in reproducing the spatial PDF of the concentration showing that the gamma distribution is the most robust and convenient model to describe the whole temporal evolution of the dispersion process. Assuming the gamma distribution as the PDF describing the scalar concentration within a given volume, we developed a simple probabilistic mixing model, that allows us to link the decay rate of the intensity of the concentration fluctuations i_c to a characteristic mixing timescale.

Finally, drawing an analogy between the present DNS results and the previous experimental data allows us to explain the similarity observed between the spatial statistics in the system considered here and the one-point statistics registered in wind-tunnel experiments. Notably, the first phase of the simulations provides a PDF that can be observed in wind-tunnel experiments by registering the concentration signal close to the source when the meandering of the plume is intense. Instead, in the second phase of the simulation when the scalar has filled the whole domain the concentration PDF corresponds to experimental PDF registered far from the source where the plume meandering is suppressed, and the plume spread is governed by the relative dispersion.

A comparison between DNS and wind-tunnel measurements of stratified turbulence will be the subject of a future investigation along the lines of the present paper. Indeed, unlike the HIT case, in the presence of stratification, sporadic extreme events develop in the vertical component of the velocity and in the temperature affecting mixing and transport properties of turbulent flows as shown in previous works [36–39].

ACKNOWLEDGMENTS

R.M. acknowledges support from the Project "EVENTFUL" (Grant No. ANR-20-CE30-0011), funded by the French "Agence Nationale de la Recherche"—ANR.

[1] K. R. Sreenivasan, Turbulent mixing: A perspective, Proc. Natl. Acad. Sci. USA **116**, 18175 (2018).
[2] E. Villermaux and J. Duplat, Mixing as an Aggregation Process, Phys. Rev. Lett. **91**, 184501 (2003).
[3] J. Bakosi, P. Franzese, and Z. Boybeyi, Probability density function modeling of scalar mixing from concentrated sources in turbulent channel flow, Phys. Fluids **19**, 115106 (2007).
[4] Q. Nguyen and D. V. Papavassiliou, A statistical model to predict streamwise turbulent dispersion from the wall at small times, Phys. Fluids **28**, 125103 (2016).

[5] P. R. Van Slooten, Jayesh, and S. B. Pope, Advances in pdf modeling for inhomogeneous turbulent flows, Phys. Fluids **10**, 246 (1998).
[6] E. Yee and A. Skvortsov, Scalar fluctuations from a point source in a turbulent boundary layer, Phys. Rev. E **84**, 036306 (2011).
[7] J. Duplat and E. Villermaux, Mixing by random stirring in confined mixtures, J. Fluid Mech. **617**, 51 (2008).
[8] D. J. Wilson and B. W. Simms, *Exposure time effects on concentration fluctuations in plumes* (Alberta Environment, 1985).
[9] M. Cassiani, The volumetric particle approach for concentration fluctuations and chemical reactions in Lagrangian particle and particle-grid models, Boundary-Layer Meteorol. **146**, 207 (2013).
[10] M. B. Bertagni, M. Marro, P. Salizzoni, and C. Camporeale, Solution for the statistical moments of scalar turbulence, Phys. Rev. Fluids **4**, 124701 (2019).
[11] M. B. Bertagni, M. Marro, P. Salizzoni, and C. Camporeale, Level-crossing statistics of a passive scalar dispersed in a neutral boundary layer, Atmos. Environ. **230**, 117518 (2020).
[12] M. Cassiani, M. Bertagni, M. Marro, and P. Salizzoni, Concentration fluctuations from localized atmospheric releases, Boundary-Layer Meteorol. **177**, 461 (2020).
[13] C. Nironi, P. Salizzoni, M. Marro, P. Mejean, N. Grosjean, and L. Soulhac, Dispersion of a passive scalar fluctuating plume in a turbulent boundary layer. Part I: Velocity and concentration measurements, Boundary-Layer Meteorol. **156**, 415 (2015).
[14] H. Ardeshiri, M. Cassiani, S. Park, A. Stohl, I. Pisso, and S. Dinger, On the convergence and capability of large eddy simulation for passive plumes concentration fluctuations in an infinite-*Re* neutral boundary layer, Boundary-Layer Meteorol. **176**, 291 (2020).
[15] P. D. Mininni, D. Rosenberg, R. Reddy, and A. Pouquet, A hybrid mpi-openmp scheme for scalable parallel pseudospectral computations for fluid turbulence, Parallel Comput. **37**, 316 (2011).
[16] See Supplemental Material at https://link.aps.org/supplemental/10.1103/PhysRevFluids.6.034502 to suitably capture the connection between the concentration pdf and the concentration fluctuations intensity i_c.
[17] S. Kullback and R. A. Leibler, On information and sufficiency, Ann. Math. Stat. **22**, 79 (1951).
[18] *Handbook of Mathematical Functions: With Formulas, Graphs, and Mathematical Tables*, edited by M. Abramowitz and I. A. Stegun, National Bureau of Standards Applied Mathematics Series (National Bureau of Standards, Washington, DC, 1965).
[19] E. Yee and R. Chan, A simple model for the probability density function of concentration fluctuations in atmospheric plumes, Atmos. Environ. **31**, 991 (1997).
[20] A. Skvortsov and E. Yee, Scaling laws of peripheral mixing of passive scalar in a wall-shear layer, Phys. Rev. E **83**, 036303 (2011).
[21] D. Oettl and E. Ferrero, A simple model to assess odour hours for regulatory purposes, Atmos. Environ. **155**, 162 (2017).
[22] M. Cassiani, P. Franzese, and U. Giostra, A PDF micromixing model of dispersion for atmospheric flow. Part I: development of the model, application to homogeneous turbulence and to neutral boundary layer, Atmos. Environ. **39**, 1457 (2005).
[23] P. G. Moschopoulos, The distribution of the sum of independent gamma random variables, Ann. Inst. Statist. Math. **37**, 541 (1985).
[24] C. H. Sim, Point processes with correlated gamma interarrival times, Stat. Probabil. Lett. **15**, 135 (1992).
[25] A. M. Mathai, Storage capacity of a dam with gamma type inputs, Ann. Inst. Statist. Math. **34**, 591 (1982).
[26] M. Akkouchi, On the convolution of gamma distributions, Soochow J. Math. **31**, 205 (2005).
[27] T. Stewart, L. W. G. Strijbosch, H. Moors, and P. van Batenburg, A simple approximation to the convolution of gamma distributions (CentER Discussion Paper, 2007).
[28] S. B. Pope, *Turbulent Flows* (Cambridge University Press, Cambridge, UK, 2011).
[29] M. Cassiani, A. Radicchi, J. Albertson, and U. Giostra, An efficient algorithm for scalar PDF modeling in incompressible turbulent flow; numerical analysis with evaluation of IEM and IECM micro-mixing models, J. Comput. Phys. **223**, 519 (2007).

[30] Z. Warhaft and J. L. Lumley, An experimental study of the decay of temperature fluctuations in grid-generated turbulence, J. Fluid Mech. **88**, 659 (1978).
[31] S. Tavoularis and S. Corrsin, Experiments in nearly homogenous turbulent shear flow with a uniform mean temperature gradient. part 1, J. Fluid Mech. **104**, 311 (1981).
[32] Z. Warhaft, Passive scalars in turbulent flows, Annu. Rev. Fluid Mech. **32**, 203 (2000).
[33] S. Heinz, *Statistical Mechanics of Turbulent Flows* (Springe-Verlag, Berlin, Heidelberg, New York, Tokyo, 2003).
[34] J. Duplat, C. Innocenti, and E. Villermaux, A nonsequential turbulent mixing process, Phys. Fluids **22**, 035104 (2010).
[35] B. L. Sawford and H. Stapountzis, Concentration fluctuations according to fluctuating plume models in one and two dimensions, Boundary-Layer Meteorol. **37**, 89 (1986).
[36] R. Marino, P. Mininni, D. Rosenberg, and A. Pouquet, Inverse cascades in rotating stratified turbulence: fast growth of large scales, Europhys. Lett. **102**, 44006 (2013).
[37] F. Feraco, R. Marino, A. Pumir, L. Primavera, P. Mininni, A. Pouquet, and D. Roesenberg, Vertical drafts and mixing in stratified turbulence: Sharp transition with froude number, Europhys. Lett. **123**, 44002 (2018).
[38] A. Pouquet, D. Rosenberg, and R. Marino, Linking dissipation, anisotropy and intermittency in rotating stratified turbulence, Phys. Fluids **31**, 105116 (2019).
[39] D. Buaria, A. Pumir, F. Feraco, R. Marino, A. Pouquet, D. Rosenberg, and L. Primavera, Single-particle lagrangian statistics from direct numerical simulations of rotating-stratified turbulence, Phys. Rev. Fluids **5**, 064801 (2020).